Dalton Transactions

PAPER

View Article Online
View Journal | View Issue

Cite this: *Dalton Trans.*, 2018, **47**, 10162

Magnetic anisotropy and relaxation behavior of six-coordinate tris(pivalato)-Co(II) and -Ni(II) complexes†

Shu-Yang Chen,[a] Hui-Hui Cui,[a] Yi-Quan Zhang, *[b] Zhenxing Wang, *[c] Zhong-Wen Ouyang,[c] Lei Chen,[d] Xue-Tai Chen, *[a] Hong Yan [a] and Zi-Ling Xue [e]

Experimental and theoretical studies of magnetic anisotropy and relaxation behavior of six-coordinate tris(pivalato)-Co(II) and -Ni(II) complexes $(NBu_4)[M(piv)_3]$ (piv = pivalate, M = Co, **1**; M = Ni, **2**), with a coordination configuration at the intermediate between an octahedron and a trigonal prism, are reported. Direct current magnetic data and high-frequency and -field EPR spectra (HFEPR) of **1** have been modeled by a general Hamiltonian considering the first-order orbital angular momentum, while the spin Hamiltonian was used to interpret the data of **2**. Both **1** and **2** show easy-axis magnetic anisotropies, which are further supported by *ab initio* calculations. Alternating current (ac) magnetic susceptibilities reveal slow magnetic relaxation at an applied dc field of 0.1 T in **1**, which is characteristic of a field-induced single-ion magnet (SIM), but **2** does not exhibit single-ion magnetic properties at 1.8 K. Detailed analyses of relaxation times show a dominant contribution of a Raman process for spin relaxation in **1**.

Received 19th April 2018,
Accepted 2nd July 2018

DOI: 10.1039/c8dt01554f

rsc.li/dalton

Introduction

Single-molecule magnets (SMMs) are molecular species that retain magnetization at low temperature after removing the external magnetic field due to the existence of an energy barrier, which prevents the reversal of magnetic moment. Such molecular nanomagnets have showed potential applications in quantum computation, high density information storage, and molecular spintronics.[1] Initially many efforts were devoted to polynuclear 3d-based SMMs.[2] More recently, SMM behaviors have also been demonstrated in metal complexes containing single paramagnetic lanthanide,[3] actinide,[4] or transition metal ions,[5] which are termed single-ion magnets (SIMs). Since the first Fe(II)-SIM complex was reported by Long *et al.* in 2010,[6] slow magnetic relaxation has been revealed in numerous d-ion complexes containing V(IV),[7] Mn(III,IV),[8] Fe(I,II,III),[6,9] Co(I,II),[10–12] Ni(I,II),[13] Cu(II),[14] Cr(II),[15] and Re(IV).[16] Co(II)-SIMs constitute the largest family because of their non-integer ground-state spin and large magnetic anisotropy.

Magnetic anisotropy is the most important factor responsible for slow magnetic relaxation. The advantage of SIMs is that magnetic anisotropy can be easily fine-tuned by the interplay between ligand field splitting and spin–orbit interactions. For the majority of d-ion complexes,[6–16] the first-order orbital momentum is usually quenched by the ligand field. Thus, magnetic anisotropy arises from the coupling between a non-degenerate electronic ground state and an orbitally degenerate excited state. Since such spin–orbital coupling is usually weak, the resulting magnetic anisotropy is mostly small, which can be modeled as zero-field splitting using axial and rhombic parameters D and E, respectively. However, in some cases where orbital momentum is unquenched or only partially quenched as in six-coordinate Co(II) complexes, the first-order spin–orbital coupling occurs and contributes to large magnetic anisotropy. In these cases, magnetic anisotropy cannot be modeled by the spin-only Hamiltonian with the D and E parameters. The mostly employed technique to probe magnetic anisotropy is magnetometry. However, in the absence of the confirmative data from other physical techniques and theoretical calculations, the reliability of the results, especially the sign of the magnetic anisotropy derived, may be questioned.

[a]*State Key Laboratory of Coordination Chemistry, School of Chemistry and Chemical Engineering, Nanjing University, Nanjing 210023, China. E-mail: xtchen@nju.edu.cn*
[b]*Jiangsu Key Laboratory for NSLSCS, School of Physical Science and Technology, Nanjing Normal University, Nanjing 210023, China. E-mail: zhangyiquan@njnu.edu.cn*
[c]*Wuhan National High Magnetic Field Center & School of Physics, Huazhong University of Science and Technology, Wuhan 430074, China. E-mail: zxwang@hust.edu.cn*
[d]*School of Environmental and Chemical Engineering, Jiangsu University of Science and Technology, Zhenjiang 212003, China*
[e]*Department of Chemistry, University of Tennessee, Knoxville, Tennessee 37996, USA*
†Electronic supplementary information (ESI) available: XRD patterns, calculation results and magnetic data. See DOI: 10.1039/c8dt01554f

Thus, a combination analysis of various techniques (*e.g.* magnetometry and HFEPR) and theoretical calculations is usually required.

The coordination configurations of the reported Co(II)-SIMs vary along with the coordination number from two to eight.[10–12] Since the first example of the six-coordinate field-induced Co(II) SIM was reported,[11a] many Co(II) complexes with octahedral[11] or trigonal prismatic geometries,[12] which exhibit slow magnetic relaxation, have been reported. Most of the six-coordinate Co(II)-complexes exhibit easy-plane magnetic anisotropy[5,11a–f] while only a few examples with easy-axis anisotropy are known.[11g–n,12] Compared with these distorted octahedral geometries,[11] a trigonal prism is a better geometry to give large easy-axis magnetic anisotropy, which results in zero-field SIMs with a high energy barrier.[12a–e] For example, Gao *et al.* reported a series of mononuclear, six-oxygen-coordinated Co(II) complexes with distorted trigonal prismatic geometries and energy barriers in the range of 26.6–102.8 cm^{-1}.[12a,b] Winpenny *et al.* revealed a Co(II) cage complex with a trigonal prismatic configuration constructed by six nitrogen atoms, showing SIM behavior with an energy barrier of 152 cm^{-1},[12c] which is relatively high among d-ion based SIMs. It is noted that the reported Co(II) complexes showing zero-field slow magnetic relaxation exhibit a trigonal prismatic geometry with a twist angle smaller than 23.5°.[11n,12]

Magnetic anisotropy of Ni(II) complexes has been studied to a lesser extent compared to Co(II) complexes.[17–19] HFEPR has been successfully used to probe the magnetic anisotropies of Ni(II) complexes of various coordination environments and geometries.[18,19] However, the examples of Ni(II)-SIMs are rare, which include two octahedral Ni(II) complexes[13b,c] and one trigonal bipyramidal Ni(II) complex.[13d]

With the aim to provide more experimental data on magnetic anisotropy dependent on the coordination geometry, we have investigated direct current (dc) and alternating current (ac) magnetic properties of two mononuclear Co(II) and Ni(II) complexes $(NBu_4)[M(piv)_3]$ (piv = pivalate, M = Co, **1**; M = Ni, **2**) with a coordination configuration at the mid-point between the octahedron and trigonal prism. The dc magnetic data and high-frequency and -field EPR spectra show their easy-axis magnetic anisotropies, which have been supported by theoretical calculations at the XMS-CASPT2 level. Alternating current magnetic susceptibility data show that **1** is a field-induced single-ion magnet, while **2** does not exhibit the SIM behavior. Furthermore, theoretical calculations have been performed to reveal the magnetostructural correlations between magnetic anisotropy and structural distortion.

Experimental section

General information

Complexes **1** and **2** were prepared according to the reported procedures.[20] Their identities were confirmed by elemental analyses (CHN) performed on an Elementar Vario ELIII elemental analyzer and infrared spectra recorded on a Tensor 27 FT-IR spectrometer using KBr pellets in the range of 400–4000 cm^{-1}. The polycrystalline samples of **1** and **2** for magnetic and HFEPR studies were characterized by powder X-ray diffraction on a Bruker D8 ADVANCE X-ray powder diffractometer in the 2θ range of 5–50° at room temperature (Fig. S1 and S2, ESI†). HFEPR experiments were performed using a spectrometer constructed at the National High Magnetic Field Laboratory, USA.[21]

Magnetic measurements

Magnetic measurements were performed on polycrystalline samples of **1** and **2** restrained in a frozen eicosane matrix using a Quantum Design SQUID VSM magnetometer. Direct current (dc) magnetic data were recorded at fields up to 7 T in the range of 2.0–300 K. Alternating current (ac) susceptibilities were measured using an oscillating ac field of 0.2 mT and ac frequencies ranging from 1 to 1000 Hz. Dc magnetic susceptibilities were corrected for diamagnetism using Pascal's constants and a sample holder correction.

Results and discussion

Structural features

The crystal structures of **1** and **2** have already been reported.[20] Their main structural aspects related to the magnetic properties are emphasized here. Their important crystal data and bond parameters are summarized in Table S1.† The structures of **1** and **2** are presented in Fig. 1. They are isostructural with the central metal ion displaying a six-coordinate geometry, in which three pivalate anions act as bidentate ligands with acute bite angles of 61.86(8), 62.18(8), and 62.00(8)° for **1** and 60.68(1), 61.48(1), and 62.54(2)° for **2**. The M–O distances are in the range of 2.105(2)–2.147(2) Å in **1** and 2.045(4)–2.108(4) Å in **2**. The six coordinated oxygen atoms can be viewed as in the parallel upper and lower planes with dihedral angles of 2.44° (**1**) and 1.79° (**2**). The twist angle φ, defined as the rotation angle of one coordination triangle away from the eclipsed configuration to the other, is 60° for an ideal octahedron and 0° for an ideal trigonal prism, respectively (Fig. 2). The value of φ is 28.71° in **1** and 28.08° for **2**, respectively, which was calculated as the average of the six torsional angles obtained by connecting skewed O atoms from different triangles *via* the centroids of the two triangles. Therefore the

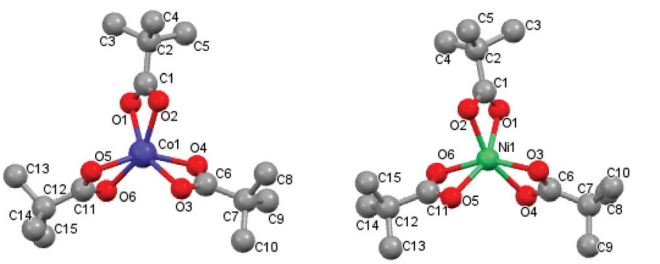

Fig. 1 Structures of the anions in **1** (left) and **2** (right).

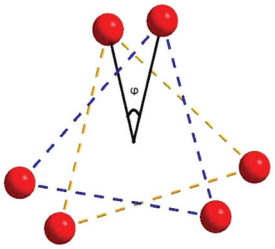

Fig. 2 Twist angle φ of the coordination polyhedron with respect to the ideal trigonal prism.

coordination geometry in both complexes can be regarded as being at the mid-point of the octahedron and trigonal prism. In order to further evaluate the degree of the structural distortion, continuous shape measurement analyses were performed using the SHAPE program.[22] The calculated value provides an estimate of the distortion degree from the possible ideal structure, and the zero value corresponds to the ideal polyhedron. The obtained values relative to the ideal octahedron and trigonal prism are 7.06 and 9.34 for **1** and 6.56 and 11.09 for **2**, respectively. The two values are rather large, suggesting the great deviations of **1** and **2** from the two ideal configurations, consistent with their intermediate coordination configuration between the octahedron and trigonal prism. The metal ions are well-separated for the shortest intermolecular M···M distances of 7.46 Å (**1**) and 7.50 Å (**2**), thus precluding any prominent intermolecular magnetic interactions.

Magnetic anisotropy of $(NBu_4)[Co(piv)_3]$ (1)

Magnetic anisotropy of **1** has been studied by dc magnetic measurements, HFEPR and theoretical calculations. Variable-temperature magnetic susceptibilities were measured for the polycrystalline sample of **1**. The resulting $\chi_M T$ *vs.* T plot shown in Fig. 3 is typical of a mononuclear Co(II) system with an orbital contribution to the magnetic moment. The $\chi_M T$ product is 3.00 cm^3 K mol^{-1} at 300 K, larger than the expected value of 1.875 cm^3 K mol^{-1} for one isolated high spin Co(II) ion center (S = 3/2, g = 2.0), indicative of the strong orbital contribution.[10–12] Upon cooling from 300 K, the $\chi_M T$ value decreases gradually to the minimum value of 1.77 cm^3 K mol^{-1} at 2.0 K. As in other six-coordinate Co(II) complexes,[11,12] such downturn indicates the presence of the strong orbital contribution, rather than the intermolecular interactions due to the long intermolecular distance between the Co(II) ions. The field-dependent magnetizations of **1** were measured from 1 to 7 T dc field at 2.0, 3.0, and 5.0 K (Fig. 3b). With the increase of the magnetic field, the magnetization continuously increases and reaches 2.25 $N_A\mu_B$ at 7 T and 2.0 K, smaller than the expected value of 3.0 $N_A\mu_B$ (g = 2.0). The high-field non-saturation also suggests the presence of significant magnetic anisotropy.

In the six-coordinate Co(II) system such as **1**, where the unquenched orbital moment contributes strongly to the magnetic moment,[23] the fitting of the magnetic data could not

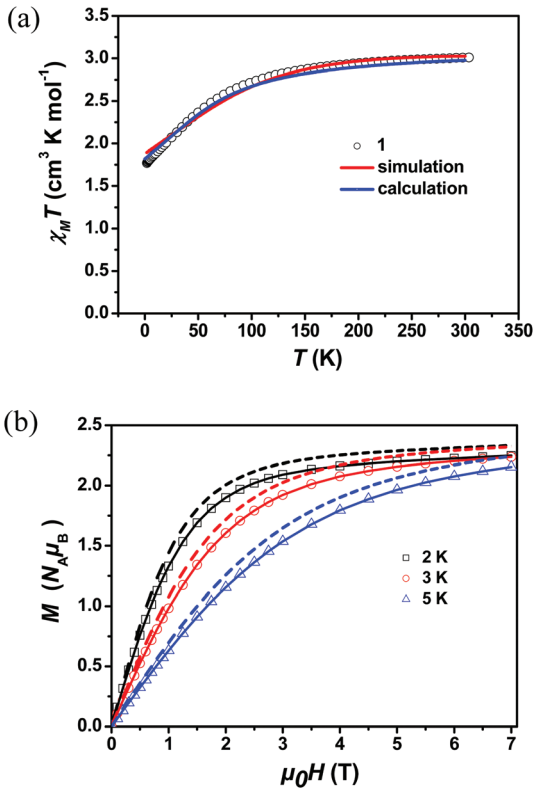

Fig. 3 (a) Variable-temperature dc susceptibility data of **1** under an applied dc field of 0.1 T. The red solid line represents the simulation using the general Hamiltonian through the PHI program[25] and the blue one is the theoretical curve calculated using the MOLCAS 8.2 program package;[27] (b) field dependent magnetizations for **1**. Solid lines are the simulations using the general Hamiltonian through the PHI program[25] while the dashed lines are the theoretical curves calculated using the MOLCAS 8.2 program package.[27]

define the sign of the magnetic anisotropy. As pointed out by Palii[11f,g] and Chilton,[11i] a joint analysis of magnetic data with other spectroscopic data such as EPR should be performed. Thus, HFEPR spectra were recorded for the polycrystalline sample of **1** at 10 K with different frequencies in the range of 50.8–428.5 GHz (Fig. 4a). All the spectra present three features, consistent with the rhombic anisotropy. A 2D resonating field *versus* frequency map containing three linear branches was derived from the observed features (Fig. 4b), indicating that these spectra can be interpreted in terms of an effective S_{eff} = 1/2 state and effective g values.[11h,i,k] The 2D map was fit[24] to give the effective g values: $g_{x,eff}$ = 2.43, $g_{y,eff}$ = 2.84 and $g_{z,eff}$ = 6.77. This pattern is consistent with the easy-axis magnetic anisotropy of **1** with significant rhombic components.

The commonly used zero-field splitting parameters D and E cannot be used to present the single-ion magnetic anisotropy in the six-coordinate Co(II) complexes with easy-axis magnetic anisotropy.[11f,g,i,23] The most trustworthy treatment of the dc magnetic data is the general Hamiltonian shown in eqn (1), which takes into account the treatment of the first-order orbital angular momentum of Co(II).

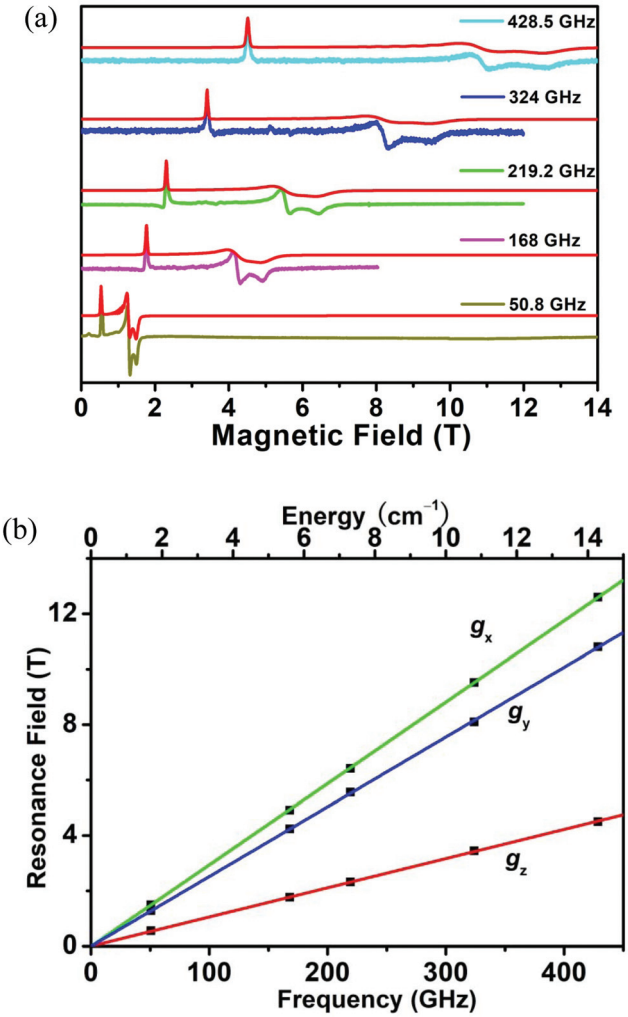

Fig. 4 (a) HFEPR spectra of **1** recorded at 10 K with various microwave frequencies. The red lines represent the simulations with the full Hamiltonian using the Hamiltonian parameters in the text using PHI;[25] (b) 2D field/frequency map of HFEPR transitions in **1**. The squares are the experimental points while green, blue, and red curves are generated by fitting using SPIN[24a] with the magnetic field *B* parallel to the *x*, *y*, and *z* axes of the ZFS tensor, respectively.

$$\hat{H} = \sigma\lambda\hat{L}\cdot\hat{S} + \sigma^2\left(B_2^0\left(3\hat{L}_z{}^2 - \hat{L}^2\right) + \frac{B_2^2}{2}\left(\hat{L}_+{}^2 + \hat{L}_-{}^2\right)\right) + \mu_B\left(\sigma\hat{L} + 2\hat{S}\right)B \quad (1)$$

where σ is the combined orbital reduction factor defined as $\sigma = -A\cdot\kappa$. The A parameter is required when using the T ≡ P equivalence for orbital triplet terms[23a,25] and takes the value of 1.0 when representing a T_2 term and 3/2 when representing a T_1 term. The κ parameter considers the reduction of the orbital momentum caused by the delocalization of the unpaired electrons. λ is the spin–orbit coupling parameter, and B_2^0 and B_2^2 are crystal field parameters (CFPs).[11i,23,25] To avoid the overparameterisation, we fix the spin–orbit coupling parameter for the Co(II) ion to $\lambda = -170$ cm^{-1} and treat both HFEPR and magnetic data with three parameters σ, B_2^0 and B_2^2. In order to reproduce the observed $g_{x,\mathrm{eff}} < g_{y,\mathrm{eff}} < g_{z,\mathrm{eff}}$ in the HFEPR spectra, B_2^0 should be negative. We found excellent agreement with the HFEPR g_{eff} values using $\sigma = 1.33$, $B_2^0 = -134.4$ cm^{-1} and $B_2^2 = 37.5$ cm^{-1} (Fig. 4a). These parameters also lead to the simulated magnetic curves, which agree well with the experimental magnetic data (Fig. 3).

In order to gain further insight into the electronic structure of **1**, theoretical calculations were carried out at the XMS-CASPT2[26] level using the MOLCAS 8.2 program package.[27] Calculation details are given in the ESI.† The energies of the spin-free states and spin–orbit states were calculated for **1**, which are listed in Tables S2–S4.† The energy difference (447.1 cm^{-1}) between the lowest two spin-free states (Table S2†) is larger than that between the lowest two spin–orbit states (167.6 cm^{-1}, Table S4†). However, the spin–orbit ground state is composed of the lowest three spin-free states, not just formed from the ground one (Table S3†). These suggest that there is very strong first-order spin–orbit coupling in **1** and zero-field splitting parameters D and E cannot be used to depict its magnetic anisotropy. The calculated $S = 1/2$ effective g-values of the ground state Kramers doublet of the Co^{II} of **1**, $g_x = 2.194$, $g_y = 3.345$, and $g_z = 6.835$, are well consistent with those of the EPR spectra. The calculated orientations of the g_x, g_y, and g_z (hard axis) of the ground doublet on the Co^{II} ion are shown in Fig. S4.† The direction of the easy axis is approximately along the C_3-axis of **1**. Furthermore, magnetic susceptibilities and magnetizations of **1** were also calculated as shown in Fig. 3, which are comparable to the experimental curves.

These results support the negative sign of magnetic anisotropy in **1**. The same negative anisotropy has been reported for the six-coordinated Co(II)-complexes with the trigonal prismatic geometry.[12]

Magnetic anisotropy of (NBu$_4$)[Ni(piv)$_3$] (2)

Direct current magnetic data were obtained for the polycrystalline sample of **2** (Fig. 5). Its $\chi_M T$ product is 1.30 cm^3 K mol^{-1} at 300 K, which is larger than the theoretical $\chi_M T$ value (1.16 cm^3 K mol^{-1}, $g = 2.15$) for the six-coordinate Ni(II) ion with largely quenched orbital moment. The $\chi_M T$ value remains roughly constant in the range of 300–20 K, and then decreases abruptly to 0.64 cm^3 K mol^{-1} at 2.0 K. The field-dependent magnetizations of **2** were measured from 1 to 7 T at 2.0, 3.0, and 5.0 K (Fig. 5b). The magnetization continuously increases with the magnetic field and reaches 2.03 $N_A\mu_B$ at 7 T at 2.0 K, close to the expected value of 2.0 $N_A\mu_B$ ($S = 1$, $g = 2.0$).

For the six-coordinate Ni(II) complex, the effective spin-Hamiltonian with the axial and rhombic zero-field splitting (ZFS) parameters as shown in eqn (2) can be used to present the magnetic anisotropy,[13,17–19]

$$\hat{H} = D(\hat{S}_z{}^2 - S(S+1)/3) + E(\hat{S}_x{}^2 - \hat{S}_y{}^2) + \mu_B g\hat{S}B \quad (2)$$

Here, μ_B denotes the Bohr magneton and D, E, S and B represent the axial and rhombic ZFS parameters, the spin, and the magnetic field vector, respectively. The $\chi_M T$ data and mag-

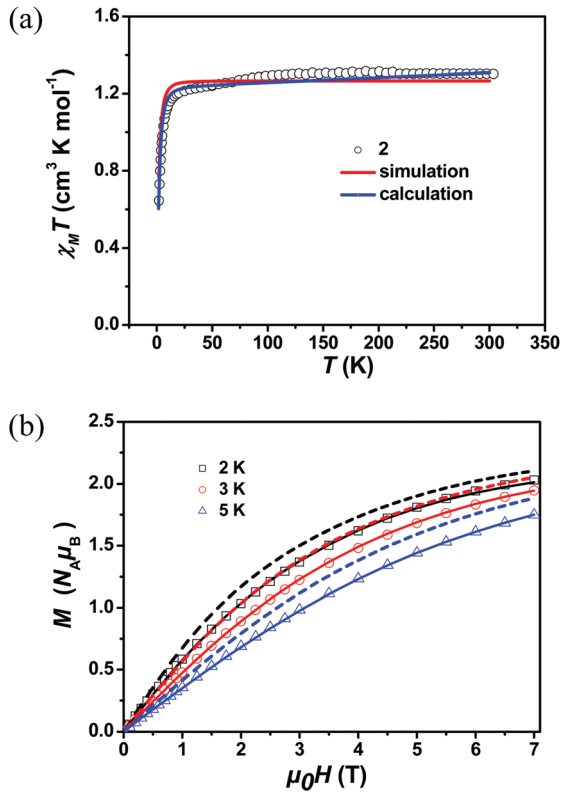

Fig. 5 (a) Variable-temperature dc susceptibility data of **2** under an applied dc field of 0.1 T. The red solid line represents the simulation using the general Hamiltonian through the PHI program[25] and the blue one is the theoretical curve calculated using the MOLCAS 8.2 program package;[27] (b) field dependent magnetizations for **2**. Solid lines are the simulations using the general Hamiltonian through the PHI program[25] while the dashed lines are the theoretical curves calculated using the MOLCAS 8.2 program package.[27]

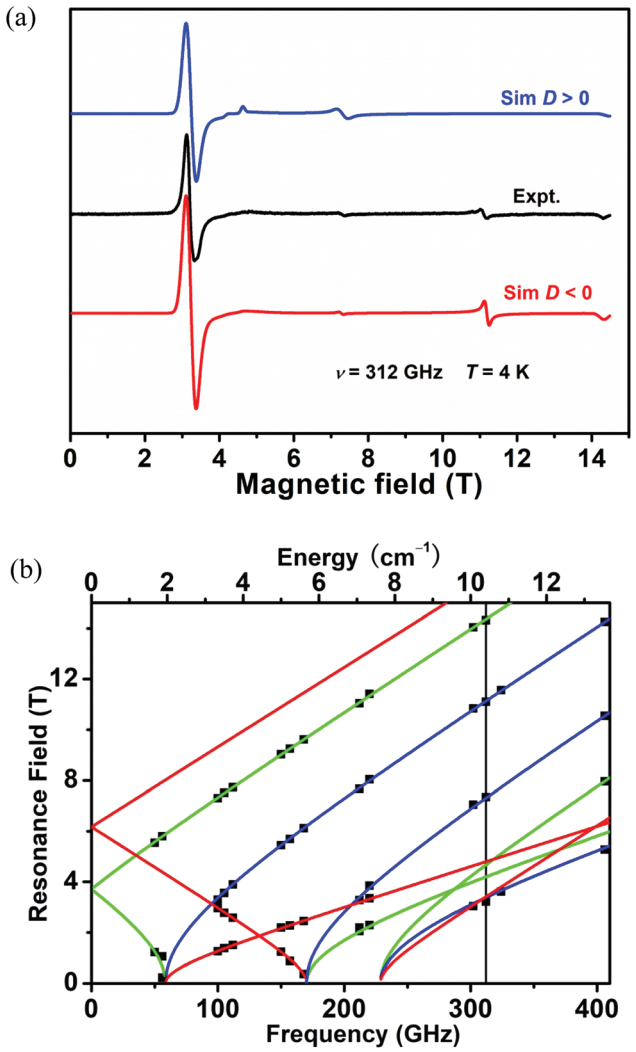

Fig. 6 (a) HF-EPR spectrum of **2** with its simulations at 312.0 GHz and 4 K (blue trace: positive *D*; red trace: negative *D*); (b) resonance field *vs.* microwave frequency of EPR transitions in **2**. The squares are the experimental points while green, blue, and red curves are generated by fittings[24a] using the spin Hamiltonian parameters indicated in the text with the magnetic field *B* parallel to the *x*, *y*, and *z* axes of the ZFS tensor, respectively. The vertical line represents the frequency (312.0 GHz) at which the spectra shown in (a) were taken.

netization curves were fit simultaneously using the PHI program.[25] The fitting gives a set of parameters $D = -7.86(4)$ cm^{-1}, $E = 0.76(2)$ cm^{-1}, $g_x = g_y = 2.440(3)$ and $g_z = 1.918(4)$.

The easy-axial type of magnetic anisotropy of Ni(II) in **2** was further studied using tunable-frequency HFEPR spectra[18a] with a frequency range from 56 to 406 GHz up to 14.5 T. The spectra are typical of an $S = 1$ spin state. An EPR spectrum recorded at 312.0 GHz and 4 K is shown in Fig. 6a. The main feature of the spectra is a very intense transition at a low field, denoted as B_{min}, and the three others being much weaker. The former is due to the off-axis turning point of the forbidden ($\Delta M_s = \pm 2$) transition, which is usually the highest peak in the triplet powder spectrum.[28] More information can be derived from the 2D resonating field *versus* the frequency map extracted from the turning points of the series of EPR spectra (Fig. 6b). All the experimental points can be simultaneously fit[24a] using the spin Hamiltonian to give the optimal parameters: $|D| = 6.65(6)$ cm^{-1}, $E = 0.98(2)$ cm^{-1}, $g_x = 2.23(2)$, $g_y = 2.24(2)$, and $g_z = 2.28(5)$. In order to reveal the sign of the *D* value, the EPR spectrum recorded at 312.0 GHz and 4 K was also simulated using the above Hamiltonian parameters. The blue and red traces are the simulated spectra using the positive and negative *D* values, respectively, which prove a negative *D* value for **2**. These parameters are also within the zero-field splitting parameters reported for the six-coordinate Ni(II) complexes determined by HFEPR techniques.[19]

The Hamiltonian parameters determined by HFEPR cannot provide good agreement with the experimental magnetic data especially the magnetization data (Fig. S5†). If the *g* values are fixed as those determined by HFEPR, the fitting of magnetic data gave *D* and *E* values being −7.78(22) and 1.38(6) cm^{-1} (Fig. S6†). Such an inconsistency between the Hamiltonian parameters from HFEPR and magnetic data is not unusual.[29] It is well known that the fitting of magnetic data would not

give the reliable Hamiltonian parameters, which could be due to the occurrence of impurities, the possible weak intermolecular interactions, the orientation of the microcrystals under the magnetic field and other undefined structures.[19f–h]

The zero-field splitting parameters of **2** were calculated at the XMS-CASPT2 level[26] using the MOLCAS 8.2 program package.[27] The calculated D, E (cm^{-1}) and the g tensor (x, y, z) of **2** are listed in Table S5,† where the calculated D (-7.1 cm^{-1}) and E (1.2 cm^{-1}) values agree well with those determined by HFEPR spectra (D = $-6.65(6)$, E = 0.98(2) cm^{-1}). The orientation of the easy axis of the ground doublet on the Ni^{II} ion is also approximately along the C_3-axis as shown in **2** (Fig. S4†). The calculated magnetic susceptibilities and magnetizations of **2** shown in Fig. 5 are comparable to the experimental curves. These results furthermore support the easy-axis magnetic anisotropy of **2**.

Magnetic relaxation by ac magnetic susceptibility studies

Alternating current susceptibility measurements were performed for **1** and **2** in order to study the low temperature dynamic magnetic behavior. No out-of-phase ac susceptibility (χ''_M) signal was observed for **1** under zero applied dc field at 1.8 K (Fig. S7a†), which is probably due to the occurrence of quantum tunneling of magnetization (QTM). The application of an external magnetic field could induce the frequency-dependent ac susceptibilities (Fig. S7a†), suggesting that the QTM phenomenon could be suppressed. For **1**, the maximum of χ''_M appears at 0.04 T, which becomes the strongest with the increasing of the applied magnetic field up to 0.1 T. Therefore an optimum magnetic field of 0.1 T was used for temperature- and frequency-dependent ac susceptibility measurements in the temperature range of 1.8–6.0 K (Fig. 7a and S8†). A frequency-dependent signal was observed below 6 K as shown in the χ''_M *vs.* T plot (Fig. S8†), suggesting field-induced slow magnetic relaxation.

In contrast with **1**, no significant χ''_M signals were observed for **2** with the frequency of 1–1000 Hz at 1.8 K under an applied magnetic field in the range of 0–0.1 T (Fig. S7b†), suggesting that **2** does not exhibit the SIM properties at 1.8 K.

The Cole–Cole plots were created from the alternating current data of **1** and fit using the generalized Debye model[30] based on eqn (3) to extract the values and distribution of the relaxation times:

$$\chi_{ac}(\omega) = \chi_S + \frac{\chi_T - \chi_S}{1 + (i\omega\tau)^{(1-\alpha)}} \quad (3)$$

where χ_T and χ_S are the isothermal and the adiabatic susceptibility, respectively; ω is the angular frequency; τ is the relaxation time; α indicates deviation from a pure Debye model.[31] As shown in Fig. S9,† the Cole–Cole plots of χ''_M *vs.* χ'_M between 1.8 and 3.4 K have semicircular profiles, indicative of a single relaxation process. The fitting parameters are summarized in Table S6.† The parameter α is in the range of 0.05–0.25 and is found to increase with the decrease of temperature, suggesting a small distribution of relaxation times.

The obtained values of relaxation time in the range of 1.8 to 3.4 K were fit using the Arrhenius law $\tau = \tau_0 \exp(U_{eff}/kT)$ to give U_{eff} = 20.7 cm^{-1} ($\tau_0 = 2.69 \times 10^{-8}$ s) for **1** (Fig. S10†). This derivation of the effective energy barrier was based on the assumption that the dominant relaxation mechanism is the thermally activated Orbach process in the studied temperature range. In fact, the Orbach mechanism is not necessarily the dominant process, at least in the investigated temperature range. The obvious curvature in the Arrhenius plot of **1** implies that the non-negligible Raman process could contribute to the relaxation rate. On this ground, a model including Orbach and Raman mechanisms was used to analyze the contribution to the relaxation rate in **1** by using eqn (4):[31]

$$\tau^{-1} = CT^n + \tau_0^{-1} \exp(-U_{eff}/kT) \quad (4)$$

Here, the two terms represent the contributions of the Raman and Orbach processes, respectively. The best fitting of the relaxation time *vs.* temperature curves gives the following parameters: n = 5.7, C = 1.1 s^{-1} $K^{-5.7}$, $\tau_0 = 1.2 \times 10^{-8}$ s, and U_{eff} = 23.1 cm^{-1}. The fit reproduces the experimental data very well (Fig. S11†). The use of the Orbach model implies that an excited state exists at an energy separation of 23.1 cm^{-1} above the ground state to provide the intermediate state for the relaxation process. But the first excited state is theoretically predicted to be 167.7 cm^{-1} higher than the ground state for **1**. Therefore, the Orbach process is unlikely to be involved in magnetic relaxation in **1**. When the Orbach mechanism is neg-

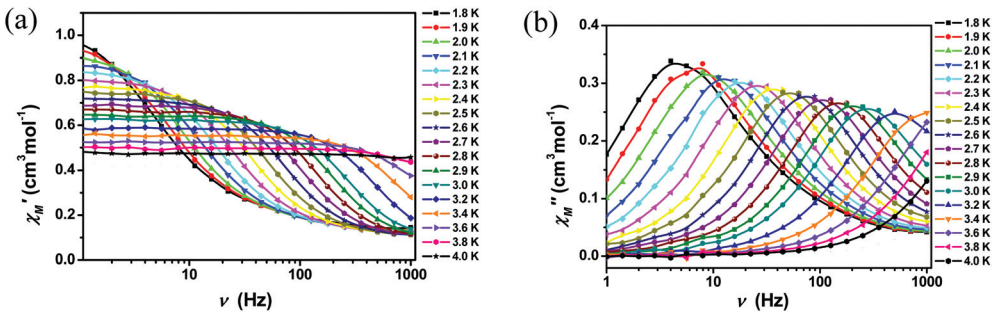

Fig. 7 Frequency dependence of the in-phase (χ'_M) (a) and out-of-phase (χ''_M) (b) ac magnetic susceptibilities from 1.8 to 4.0 K under 0.1 T dc field for **1**. The solid lines are a guide to the eye.

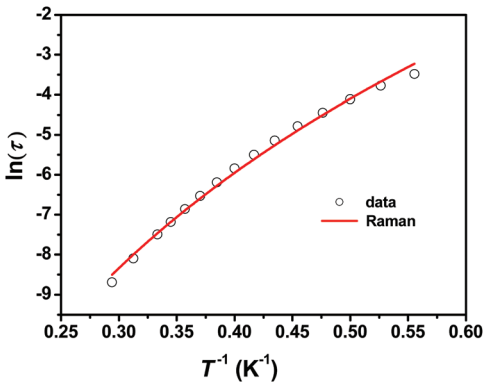

Fig. 8 ln(τ) *vs.* T^{-1} plot of complex **1**.

lected, the relaxation time data could be fit using a power law $\tau^{-1} = CT^n$ to give the resulting values n = 8.3 and C = 0.19 s^{-1} $K^{-8.3}$ (Fig. 8). The obtained n value is very close to the expected n = 9 for the Raman mechanism in Kramers ions, suggesting the dominant contribution of a Raman process for the spin relaxation in **1**.[31]

Theoretical studies on magnetostructural correlations

Several reported Co(II) complexes showing zero-field slow magnetic relaxation exhibit a distorted trigonal prismatic geometry with a twist angle smaller than 23.5°.[11n,12] Complex **1** displaying slow magnetic relaxation under a magnetic field has a twist angle of 28.7°. Dunbar and Song *et al.* reported field-induced slow magnetic relaxation in several Co(II) complexes with a trigonal antiprismatic configuration with twist angles close to 60°.[11l–n] To gain further insight into magnetic anisotropies in tris(pivalato)-Co(II) and -Ni(II) complexes, we carried out further theoretical studies on a series of model complexes with the twist angle φ from 0 to 60° by rotating the one O3 plane relative to the other. For each model complex of Co(II), the energy level and the $\boldsymbol{g}$ tensor of the ground and first excited doublets of the Co(II) ion were calculated using XMS-CASPT2[26] with MOLCAS 8.2.[27] The calculation results are summarized in Fig. 9 and Table S7.† When the twist angle φ is zero, corresponding to a trigonal prismatic geometry, g_x and g_y values are nearly zero and g_z is 9.572, which is of highly axial anisotropy. When the φ becomes larger, the g_x and g_y increase but g_z decreases, reaching a cross-over point at about 35°, where three g values are identical. Upon further increasing the φ angle, g_x and g_y become larger than g_z, showing the easy-plane anisotropy. These trends lead to an important conclusion that the Co(II) ion exhibits easy-axis magnetic anisotropy when a twist angle is smaller than 35° while positive anisotropy is found with a twist angle larger than 35°. A similar crossover from easy-axis to easy-plane anisotropy has been predicted in a CoN_6 system.[12e] Furthermore, the increase of g_x and g_y with φ suggests the enhanced transversal anisotropy in Co(II). In **1** with a twist angle φ of 28.7°, the quantum tunnelling of magnetization (QTM) induced by a transversal magnetic field ($2\Delta_{tun} = \mu_B[g_x^2H_x^2 + g_y^2H_y^2]^{1/2}$) might be strong.[32] Moreover, the discrepancy between g_x and g_y in **1** also promotes the QTM. Thus, no slow magnetic relaxation is

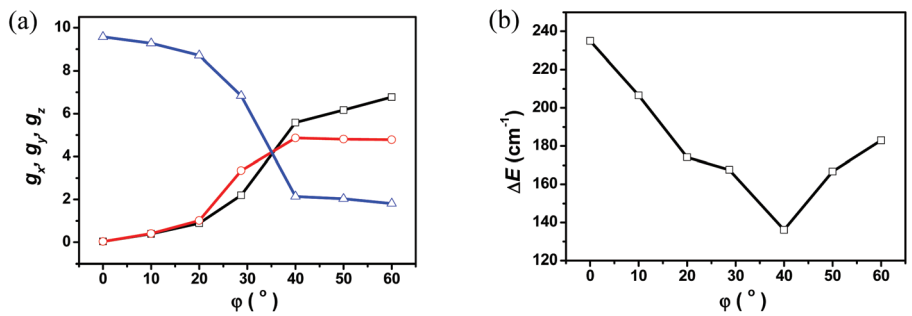

Fig. 9 The correlation between the twist angle φ (°) and g_x (black), g_y (red), and g_z (blue) (a) and the energy gap (cm^{-1}) (b) in Co(II) complexes.

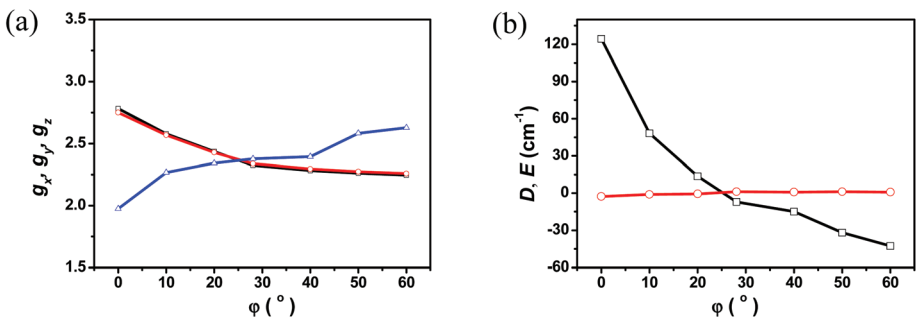

Fig. 10 The correlation between the twist angle φ (°) and g_x (black), g_y (red), and g_z (blue) (a) and D (black) and E (red) (b) in Ni(II) complexes.

observed in **1** under zero field. Accompanied by the above trend, the energy gap between the ground and the first excited state also varies with φ (Fig. 10b). With the increase of φ from zero, the energy gap decreases and reaches a minimum at 40° and then increases again. The minimum value corresponds to the cross-over point.

The g values and zero field splitting parameters D and E were calculated for a series of model complexes with different twist angles derived from **2**, which are summarized in Fig. 10 and Table S8.† When the twist angle φ increases from zero, the Ni(II) complex exhibits easy-plane anisotropy and then easy-axis anisotropy through a crossover point at the twist angle of *ca.* 25°. Our complex **2** is nearly at the cross-over point and has a small negative D value, which could be the reason why no slow magnetic relaxation was observed for **2** even under a magnetic field. From the comparison of the above calculated results of the model complexes based on **1** and **2**, we can conclude that at the two extremes of the coordination configuration, *i.e.* trigonal prism geometry or trigonal antiprism, Co(II) and Ni(II) complexes would exhibit the opposite anisotropy. To have large and negative anisotropy, the trigonal prism is a better choice for Co(II) while the trigonal antiprism is the choice for Ni(II).

Conclusions

The static and dynamic magnetic studies have been performed on mononuclear, six-coordinated Co(II) and Ni(II) complexes $(NBu_4)[M(piv)_3]$ (piv = pivalate, M = Co, **1**; M = Ni, **2**) with a configuration at the midpoint between the octahedron and trigonal prism. The joint studies employing magnetic measurements, HFEPR spectroscopy and theoretical calculations confirm the negative sign of magnetic anisotropy in **1** and **2**. The ac magnetic susceptibility data show that **1** is a field-induced SIM, but **2** does not show slow magnetic relaxation at 1.8 K. While the six-coordinate Co(II) complexes with positive magnetic anisotropy are well studied, the examples of the complexes exhibiting field-induced SIM properties due to the negative magnetic anisotropy are relatively scarce. This work adds a new number of six-coordinate Co(II)-based field-induced SIM with negative magnetic anisotropy.

The magnetic anisotropies of **1** and **2** and those model complexes with different twist angles have been theoretically studied. The trigonal prismatic geometry is found to be a better choice for larger and negative anisotropy of six-coordinate Co(II), which is consistent with that reported in experimental and theoretical studies.[12] But our calculations predict that Ni(II) complexes with the trigonal antiprism would exhibit large easy-axis anisotropy.

Conflicts of interest

There are no conflicts to declare.

Acknowledgements

We are grateful for the financial support from the Natural Science Grant of China (No. 21471078 to XTC, and 11774178 to YQZ), and the US National Science Foundation (CHE-1633870 to ZLX). The National High Magnetic Field Laboratory is funded by the National Science Foundation *via* Cooperative Agreement No. DMR-1157490 and the State of Florida.

Notes and references

1 (*a*) D. Gatteschi and R. Sessoli, *Angew. Chem., Int. Ed.*, 2003, **42**, 268; (*b*) W. Wernsdorfer and R. Sessoli, *Science*, 1999, **284**, 133; (*c*) M. N. Leuenberger and D. Loss, *Nature*, 2001, **410**, 789; (*d*) R. E. P. Winpenny, *Angew. Chem., Int. Ed.*, 2008, **47**, 7992; (*e*) D. Gatteschi, R. Sessoli and J. Villain, *Molecular Nanomagnets*, Oxford University Press, Oxford, UK, 2006.

2 (*a*) R. Sessoli, H. L. Tsai, A. R. Schake, S. Wang, J. B. Vincent, K. Folting, D. Gatteschi, G. Christou and D. N. Hendrickson, *J. Am. Chem. Soc.*, 1993, **115**, 1804; (*b*) R. Sessoli, D. Gatteschi, A. Caneschi and M. A. Novak, *Nature*, 1993, **365**, 141; (*c*) R. Bagai and G. Christou, *Chem. Soc. Rev.*, 2009, **38**, 1011; (*d*) D. Gatteschi, R. Sessoli and A. Cornia, *Chem. Commun.*, 2000, 725; (*e*) K. S. Pedersen, J. Bendix and R. Clérac, *Chem. Commun.*, 2014, **50**, 4396; (*f*) M. Murrie, *Chem. Soc. Rev.*, 2010, **39**, 1986.

3 (*a*) D. N. Woodruff, R. E. P. Winpenny and R. A. Layfield, *Chem. Rev.*, 2013, **113**, 5110; (*b*) H. L. C. Feltham and S. Brooker, *Coord. Chem. Rev.*, 2014, **276**, 1.

4 N. Magnani and R. Caciuffo, *Inorganics*, 2018, **6**, 26.

5 (*a*) G. A. Craig and M. Murrie, *Chem. Soc. Rev.*, 2015, **44**, 2135; (*b*) A. K. Bar, C. Pichon and J.-P. Sutter, *Coord. Chem. Rev.*, 2016, **308**, 346; (*c*) J. M. Frost, K. L. M. Harriman and M. Murugesu, *Chem. Sci.*, 2016, **7**, 2470; (*d*) M. Atanasov, D. Aravena, E. Suturina, E. Bill, D. Maganas and F. Neese, *Coord. Chem. Rev.*, 2015, **289–290**, 177; (*e*) S. Gómez-Coca, D. Aravena, R. Morales and E. Ruiz, *Coord. Chem. Rev.*, 2015, **289–290**, 379.

6 D. E. Freedman, W. H. Harman, T. D. Harris, G. J. Long, C. J. Chang and J. R. Long, *J. Am. Chem. Soc.*, 2010, **132**, 1224.

7 M. Atzori, L. Tesi, E. Morra, M. Chiesa, L. Sorace and R. Sessoli, *J. Am. Chem. Soc.*, 2016, **138**, 2154.

8 (*a*) J. Vallejo, A. Pascual-Álvarez, J. Cano, I. Castro, M. Julve, F. Lloret, J. Krzystek, G. D. Munno, D. Armentano, W. Wernsdorfer, R. Ruiz-García and E. Pardo, *Angew. Chem., Int. Ed.*, 2013, **52**, 14075; (*b*) M. Ding, G. E. Cutsail III, D. Aravena, M. Amoza, M. Rouzières, P. Dechambenoit, Y. Losovyj, M. Pink, E. Ruiz, R. Clérac and J. M. Smith, *Chem. Sci.*, 2016, **7**, 6132.

9 (*a*) J. M. Zadrozny, D. J. Xiao, M. Atanasov, G. J. Long, F. Grandjean, F. Neese and J. R. Long, *Nat. Chem.*, 2013, **5**, 577; (*b*) M. Atanasov, J. M. Zadrozny, J. R. Long and

F. Neese, *Chem. Sci.*, 2013, **4**, 139; (*c*) A. K. Bar, C. Pichon, N. Gogoi, C. Duhayon, S. Ramasesha and J.-P. Sutter, *Chem. Commun.*, 2015, **51**, 3616; (*d*) S. Mossin, B. L. Tran, D. Adhikari, M. Pink, F. W. Heinemann, J. Sutter, R. K. Szilagyi, K. Meyer and D. J. Mindiola, *J. Am. Chem. Soc.*, 2012, **134**, 13651.

10 (*a*) Y.-S. Meng, Z. Mo, B.-W. Wang, Y.-Q. Zhang, L. Deng and S. Gao, *Chem. Sci.*, 2015, **6**, 7156; (*b*) X.-N. Yao, J.-Z. Du, Y.-Q. Zhang, X.-B. Leng, M.-W. Yang, S.-D. Jiang, Z.-X. Wang, Z.-W. Ouyang, L. Deng, B.-W. Wang and S. Gao, *J. Am. Chem. Soc.*, 2017, **139**, 373; (*c*) A. Eichhöfer, Y. Lan, V. Mereacre, T. Bodenstein and F. Weigend, *Inorg. Chem.*, 2014, **53**, 1962; (*d*) S. Gomez-Coca, E. Cremades, N. Aliaga-Alcalde and E. Ruiz, *J. Am. Chem. Soc.*, 2013, **135**, 7010; (*e*) F. Habib, O. R. Luca, V. Vieru, M. Shiddiq, I. Korobkov, S. I. Gorelsky, M. K. Takase, L. F. Chibotaru, S. Hill, R. H. Crabtree and M. Murugesu, *Angew. Chem., Int. Ed.*, 2013, **52**, 11290; (*f*) D. Schweinfurth, M. G. Sommer, M. Atanasov, S. Demeshko, S. Hohloch, F. Meyer, F. Neese and B. Sarkar, *J. Am. Chem. Soc.*, 2015, **137**, 1993; (*g*) P. Antal, B. Drahoš, R. Herchel and Z. Trávníček, *Inorg. Chem.*, 2016, **55**, 5957; (*h*) L. Chen, H.-H. Cui, S. E. Stavretis, S. C. Hunter, Y.-Q. Zhang, X.-T. Chen, Y.-C. Sun, Z. Wang, Y. Song, A. A. Podlesnyak, Z.-W. Ouyang and Z.-L. Xue, *Inorg. Chem.*, 2016, **55**, 12603; (*i*) L. Chen, J. Wang, J.-M. Wei, W. Wernsdorfer, X.-T. Chen, Y.-Q. Zhang, Y. Song and Z.-L. Xue, *J. Am. Chem. Soc.*, 2014, **136**, 12213.

11 (*a*) J. Vallejo, I. Castro, R. Ruiz-García, J. Cano, M. Julve, F. Lloret, G. De Munno, W. Wernsdorfer and E. Pardo, *J. Am. Chem. Soc.*, 2012, **134**, 15704; (*b*) E. Colacio, J. Ruiz, E. Ruiz, E. Cremades, J. Krzystek, S. Carretta, J. Cano, T. Guidi, W. Wernsdorfer and E. K. Brechin, *Angew. Chem., Int. Ed.*, 2013, **52**, 9130; (*c*) S. Gómez-Coca, A. Urtizberea, E. Cremades, P. J. Alonso, A. Camón, E. Ruiz and F. Luis, *Nat. Commun.*, 2014, **5**, 4300; (*d*) R. Herchel, L. Váhovská, I. Potočňák and Z. Trávníček, *Inorg. Chem.*, 2014, **53**, 5896; (*e*) R. Díaz-Torres, M. Menelaou, O. Roubeau, A. Sorrenti, G. Brandariz-de-Pedro, E. C. Saňudo, S. J. Teat, J. Fraxedas, E. Ruiz and N. Aliaga-Alcalde, *Chem. Sci.*, 2016, **7**, 2793; (*f*) A. V. Palii, D. V. Korchagin, E. A. Yureva, A. V. Akimov, E. Y. Misochko, G. V. Shilov, A. D. Talantsev, R. B. Morgunov, S. M. Aldoshin and B. S. Tsukerblat, *Inorg. Chem.*, 2016, **55**, 9696; (*g*) D. V. Korchagin, A. V. Palii, E. A. Yureva, A. V. Akimov, E. Y. Misochko, G. V. Shilov, A. D. Talantsev, R. B. Morgunov, A. A. Shakin, S. M. Aldoshin and B. S. Tsukerblat, *Dalton Trans.*, 2017, **46**, 7540; (*h*) A. Świtlicka-Olszewska, J. Palion-Gazda, T. Klemens, B. Machura, J. Vallejo, J. Cano, F. Lloret and M. Julve, *Dalton Trans.*, 2016, **45**, 10181; (*i*) J. P. S. Walsh, G. Bowling, A.-M. Ariciu, N. F. M. Jailani, N. F. Chilton, P. G. Waddell, D. Collison, F. Tuna and L. J. Higham, *Magnetochemistry*, 2016, **2**, 23; (*j*) L. Chen, J. Zhou, H.-H. Cui, A.-H. Yuan, Z. Wang, Y.-Q. Zhang, Z.-W. Ouyang and Y. Song, *Dalton Trans.*, 2018, **47**, 2506; (*k*) E. A. Buvaylo, V. N. Kokozay, O. Y. Vassilyeva, B. W. Skelton, A. Ozarowski, J. Titiš, B. Vranovičová and R. Boča, *Inorg. Chem.*, 2017, **56**, 6999; (*l*) J. Li, Y. Han, F. Cao, R.-M. Wei, Y.-Q. Zhang and Y. Song, *Dalton Trans.*, 2016, **45**, 9279; (*m*) Y.-Z. Zhang, S. Gómez-Coca, A. J. Brown, M. R. Saber, X. Zhang and K. R. Dunbar, *Chem. Sci.*, 2016, **7**, 6519; (*n*) J. Zhang, J. Li, C. Yuan, Y.-Q. Zhang and Y. Song, *Inorg. Chem.*, 2018, **57**, 3803.

12 (*a*) Y.-Y. Zhu, C. Cui, Y.-Q. Zhang, J.-H. Jia, X. Guo, C. Gao, K. Qian, S.-D. Jiang, B.-W. Wang, Z.-M. Wang and S. Gao, *Chem. Sci.*, 2013, **4**, 1802; (*b*) Y.-Y. Zhu, Y.-Q. Zhang, T.-T. Yin, C. Gao, B.-W. Wang and S. Gao, *Inorg. Chem.*, 2015, **54**, 5475; (*c*) V. V. Novikov, A. A. Pavlov, Y. V. Nelyubina, M.-E. Boulon, O. A. Varzatskii, Y. Z. Voloshin and R. E. P. Winpenny, *J. Am. Chem. Soc.*, 2015, **137**, 9792; (*d*) A. A. Pavlov, Y. V. Nelyubina, S. V. Kats, L. V. Penkova, N. N. Efimov, A. O. Dmitrienko, A. V. Vologzhanina, A. S. Belov, Y. Z. Voloshin and V. V. Novikov, *J. Phys. Chem. Lett.*, 2016, **7**, 4111; (*e*) T. J. Ozumerzifon, I. Bhowmick, W. C. Spaller, A. K. Rappe and M. P. Shores, *Chem. Commun.*, 2017, **53**, 4211; (*f*) Y. Peng, T. Bodenstein, K. Fink, V. Mereacre, C. E. Ansona and A. K. Powell, *Phys. Chem. Chem. Phys.*, 2016, **18**, 30135; (*g*) S. Gomez-Coca, E. Cremades, N. Aliaga-Alcalde and E. Ruiz, *J. Am. Chem. Soc.*, 2013, **135**, 7010.

13 (*a*) W. Lin, T. Bodenstein, V. Mereacre, K. Fink and A. Eichhöfer, *Inorg. Chem.*, 2016, **55**, 2091; (*b*) J. Miklovič, D. Valigura, R. Boča and J. Titiš, *Dalton Trans.*, 2015, **44**, 12484; (*c*) D. Lomjanský, J. Moncol', C. Rajnák, J. Titiš and R. Boča, *Chem. Commun.*, 2017, **53**, 6930; (*d*) K. E. R. Marriott, L. Bhaskaran, C. Wilson, M. Medarde, S. T. Ochsenbein, S. Hill and M. Murrie, *Chem. Sci.*, 2015, **6**, 6823.

14 R. Boča, C. Rajnák, J. Titiš and D. Valigura, *Inorg. Chem.*, 2017, **56**, 1478.

15 (*a*) Y.-F. Deng, T. Han, Z. Wang, Z. Ouyang, B. Yin, Z. Zheng, J. Krzystek and Y.-Z. Zheng, *Chem. Commun.*, 2015, **51**, 17688; (*b*) A. Cornia, L. Rigamonti, S. Boccedi, R. Clérac, M. Rouzières and L. Sorace, *Chem. Commun.*, 2014, **50**, 15191.

16 (*a*) J. Martínez-Lillo, T. F. Mastropietro, E. Lhotel, C. Paulsen, J. Cano, G. D. Munno, J. Faus, F. Lloret, M. Julve, S. Nellutla and J. Krzystek, *J. Am. Chem. Soc.*, 2013, **135**, 13737; (*b*) K. S. Pedersen, M. Sigrist, M. A. Sørensen, A.-L. Barra, T. Weyhermiiller, S. Piligkos, C. A. Thuesen, M. G. Vinum, H. Mutka, H. Weihe, R. Clérac and J. Bendix, *Angew. Chem., Int. Ed.*, 2014, **53**, 1351.

17 (*a*) S.-D. Jiang, D. Maganas, N. Levesanos, E. Ferentinos, S. Haas, K. Thirunavukkuarasu, J. Krzystek, M. Dressel, L. Bogani, F. Neese and P. Kyritsis, *J. Am. Chem. Soc.*, 2015, **137**, 12923; (*b*) S. Gómez-Coca, E. Cremades, N. Aliaga-Alcalde and E. Ruiz, *Inorg. Chem.*, 2014, **53**, 676; (*c*) R. Ruamps, R. Maurice, L. Batchelor, M. Boggio-Pasqua, R. Guillot, A. L. Barra, J. Liu, E.-E. Bendeif, S. Pillet, S. Hill, T. Mallah and N. Guihéry, *J. Am. Chem. Soc.*, 2013, **135**, 3017; (*d*) R. Ruamps, L. J. Batchelor, R. Maurice, N. Gogoi, P. Jiménez-Lozano, N. Guihéry, C. de Graaf, A.-L. Barra,

J.-P. Sutter and T. Mallah, *Chem. – Eur. J.*, 2013, **19**, 950; (*e*) I. Nemec, R. Herchel, I. Svoboda, R. Boča and Z. Trávníček, *Dalton Trans.*, 2015, **44**, 9551.

18 (*a*) J. Krzystek, S. A. Zvyagin, A. Ozarowski, S. Trofimenko and J. Telser, *J. Magn. Reson.*, 2006, **178**, 174; (*b*) J. Krzystek, J.-H. Park, M. W. Meisel, M. A. Hitchman, H. Stratemeier, L.-C. Brunel and J. Telser, *Inorg. Chem.*, 2002, **41**, 4478; (*c*) P. J. Desrochers, J. Telser, S. A. Zvyagin, A. Ozarowski, J. Krzystek and D. A. Vicic, *Inorg. Chem.*, 2006, **45**, 8930; (*d*) I. Nieto, R. P. Bontchev, A. Ozarowski, D. Smirnov, J. Krzystek, J. Telser and J. M. Smith, *Inorg. Chim. Acta*, 2009, **362**, 4449; (*e*) J.-N. Rebilly, G. Charron, E. Rivière, R. Guillot, A.-L. Barra, M. D. Serrano, J. van Slageren and T. Mallah, *Chem. – Eur. J.*, 2008, **14**, 1169; (*f*) B. Cahier, M. Perfetti, G. Zakhia, D. Naoufal, F. El-Khatib, R. Guillot, E. Riviére, R. Sessoli, A.-L. Barra, N. Guihéry and T. Mallah, *Chem. – Eur. J.*, 2017, **23**, 3648.

19 (*a*) J. Krzystek, A. Ozarowski and J. Telser, *Coord. Chem. Rev.*, 2006, **250**, 2308; (*b*) G. Rogez, J.-N. Rebilly, A.-L. Barra, L. Sorace, G. Blondin, N. Kirchner, M. Duran, J. van Slageren, S. Parsons, L. Ricard, A. Marvilliers and T. Mallah, *Angew. Chem., Int. Ed.*, 2005, **44**, 1876; (*c*) D. Dobrzyńska, L. B. Jerzykiewicz, M. Duczmal, A. Wojciechowska, K. Jabłońska, J. Palus and A. Ozarowski, *Inorg. Chem.*, 2006, **45**, 10479; (*d*) G. Charron, F. Bellot, F. Cisnetti, G. Pelosi, J.-N. Rebilly, E. Rivère, A.-L. Barra, T. Mallah and C. Policar, *Chem. – Eur. J.*, 2007, **13**, 2774; (*e*) A. Wojciechowska, M. Daszkiewicz, Z. Staszak, A. Trusz-Zdybek, A. Bieńko and A. Ozarowskiz, *Inorg. Chem.*, 2011, **50**, 11532; (*f*) D. Maganas, J. Krzystek, E. Ferentinos, A. M. Whyte, N. Robertson, V. Psycharis, A. Terzis, F. Neese and P. Kyritsis, *Inorg. Chem.*, 2012, **51**, 7218; (*g*) D. Schweinfurth, J. Krzystek, I. Schapiro, S. Demeshko, J. Klein, J. Telser, A. Ozarowski, C.-Y. Su, F. Meyer, M. Atanasov, F. Neese and B. Sarkar, *Inorg. Chem.*, 2013, **52**, 6880; (*h*) A. Wojciechowska, J. Janczak, Z. Staszak, M. Duczmal, W. Zierkiewicz, J. Tokar and A. Ozarowski, *New J. Chem.*, 2015, **39**, 6813; (*i*) G. Charron, E. Malkin, G. Rogez, L. J. Batchelor, S. Mazerat, R. Guillot, N. Guihéry, A.-L. Barra, T. Mallah and H. Bolvin, *Chem. – Eur. J.*, 2016, **22**, 16850.

20 (*a*) E. Fursova, G. Romanenko, R. Sagdeev and V. Ovcharenko, *Polyhedron*, 2014, **81**, 27; (*b*) E. Fursova, G. Romanenko and V. Ovcharenko, *Polyhedron*, 2013, **62**, 274.

21 (*a*) B. Cage, A. Hassan, L. Pardi, J. Krzystek, L. C. Brunel and N. S. Dalal, *J. Magn. Reson.*, 1997, **124**, 495; (*b*) A. Hassan, L. Pardi, J. Krzystek, A. Sienkiewicz, P. Goy, M. Rohrer and L. C. Brunel, *J. Magn. Reson.*, 2000, **142**, 300.

22 (*a*) M. Llunell, D. Casanova, J. Cirera, P. Alemany and S. Alvarez, *Shape Program, Version 2.1*, 2013; (*b*) S. Alvarez, P. Alemany, D. Casanova, J. Cirera, M. Llunell and D. Avnir, *Coord. Chem. Rev.*, 2005, **249**, 1693.

23 (*a*) F. Lloret, M. Julve, J. Cano, R. Ruiz-García and E. Pardo, *Inorg. Chim. Acta*, 2008, **361**, 3432; (*b*) J. Titiš and R. Boča, *Inorg. Chem.*, 2011, **50**, 11838.

24 (*a*) Simulations were performed using SPIN developed by Andrew Ozarowski at the National High Magnetic Field Laboratory, USA; (*b*) F. R. Xavier, A. Neves, A. Casellato, R. A. Peralta, A. J. Bortoluzzi, B. Szpoganicz, P. C. Severino, H. Terenzi, Z. Tomkowicz, S. Ostrovsky, W. Haase, A. Ozarowski, J. Krzystek, J. Telser, G. Schenk and L. R. Gahan, *Inorg. Chem.*, 2009, **48**, 7905.

25 (*a*) N. F. Chilton, R. P. Anderson, L. D. Turner, A. Soncini and K. S. Murray, *J. Comput. Chem.*, 2013, **34**, 1164; (*b*) N. F. Chilton, *PHI User Manual v3*, 2018.

26 L. Ungur and L. F. Chibotaru, *Chem. – Eur. J.*, 2017, **23**, 3708.

27 G. Karlström, R. Lindh, P.-Å. Malmqvist, B. O. Roos, U. Ryde, V. Veryazov, P.-O. Widmark, M. Cossi, B. Schimmelpfennig, P. Neogrady and L. Seijo, *Comput. Mater. Sci.*, 2003, **28**, 222.

28 F. E. Mabbs and D. Collison, *Electron Paramagnetic Resonance of Transition Metal Compounds*, Elsevier, Amsterdam, 1992.

29 J. Krzystek and J. Telser, *Dalton Trans.*, 2016, **45**, 16751.

30 (*a*) Y.-N. Guo, G.-F. Xu, Y. Guo and J. Tang, *Dalton Trans.*, 2011, **40**, 9953; (*b*) K. S. Cole and R. H. Cole, *J. Chem. Phys.*, 1941, **9**, 341.

31 (*a*) R. L. Carlin and A. J. van Duyneveldt, *Magnetic Properties of Transition Metal compounds*, Springer-Verlag, New York, 1976; (*b*) K. N. Shrivastava, *Phys. Status Solidi B*, 1983, **117**, 437.

32 L. Ungur and L. F. Chibotaru, *Inorg. Chem.*, 2016, **55**, 10043.